

## HEALTH AND MEDICINE

# Engineering human megakaryocytic microparticles for targeted delivery of nucleic acids to hematopoietic stem and progenitor cells

Chen-Yuan Kao<sup>1,2</sup> and Eleftherios T. Papoutsakis<sup>1,2,3\*</sup>

Hematopoietic stem and progenitor cells (HSPCs) are important target cells for gene therapy applications. Current genetic modifications of HSPCs rely on viral vectors *in vivo* or electroporation *ex vivo*. Here, we developed a non-viral system based on megakaryocytic microparticles (MPs) for targeted delivery of plasmid DNA (pDNA) and small RNAs to HSPCs. We have previously shown that megakaryocytic MPs, the most abundant MPs in blood circulation, target specifically and deliver cargo to HSPCs both *in vitro* and *in vivo*. With an optimized electroporation protocol, an average of 4200 plasmid copies per MP were loaded into MP, thus enabling effective delivery of green fluorescent protein (GFP)-encoding pDNA to HSPCs and HSPC nuclei, with up to 81% nuclei containing pDNA. Effective functional small interfering RNA (siRNA) and microRNA (miRNA) delivery were also demonstrated. As patient-specific or generic megakaryocytic MPs can be readily generated and stored frozen, our data suggest that this system has great potential for therapeutic applications targeting HSPCs.

## INTRODUCTION

Cell-derived microparticles (MPs) are 0.1- to 1- $\mu\text{m}$  extracellular vesicles (EVs) generated by most, if not all, mammalian cells (1–3). MPs bud off from cellular plasma membranes under normal physiological or pathophysiological conditions (4). MPs and the smaller nanosize EVs, exosomes (<0.1  $\mu\text{m}$  and of different ontogeny), play an important role in cell-to-cell communication and transferring of materials such as RNA, proteins, or lipids to target cells (2, 5). EVs have promising characteristics for RNA, DNA, and protein and other cargo delivery, including their natural capacity to transfer cargo to target cells (2); simple and natural generation from all mammalian cells (2, 5); stable biological activity under  $-80^{\circ}\text{C}$  long-term storage (6); and, if EVs are from autologous or compatible cells, low immunogenicity and toxicity (7). Recent studies have demonstrated mRNA (8), microRNA (miRNA) (9), small interfering RNA (siRNA) (10), and drug (11, 12) delivery using naturally generated or engineered EVs.

Two main approaches for loading EVs with synthetic cargo have been investigated. Earlier studies used endogenous loading, whereby EV-producing cells were transfected with plasmid DNA (pDNA) or mRNA to overexpress specific genes, assuming that this will lead to encapsulation of nucleic acids in the EVs during their biogenesis (13). More recent investigations have focused on exogenous cargo loading. Organic molecule drugs can be loaded into EVs by simple incubation (12). Several studies used electroporation to load RNAs or drugs to EVs (10, 11, 14–16). Most studies used cancer cell line-derived exosomes, not MPs, and very few examined DNA delivery (16, 17). Linear double-stranded DNA (dsDNA) [750 base pairs (bp)] via human embryonic kidney (HEK) 293T-derived 85-nm exosomes was delivered to the same cell type, but loading linear dsDNA larger than 1000 bp to these exosomes was inefficient, while loading pDNA was practically impossible due to the small size of exosomes (16). Kanada *et al.* (17) examined cargo delivery, both *in vitro* and *in vivo*, by HEK293FT-

derived exosomes and MPs to show that functional protein expression was only possible from MP-mediated pDNA delivery.

Efficient methods to deliver cargo to hematopoietic stem and progenitor cells (HSPCs) are important not only for fundamental studies of hematopoietic disorders and malignancies but also for therapeutic applications. Current approaches, including viral and nonviral methods, for cargo (DNA, RNA, or protein) delivery to HSPCs have substantial limitations (18–20). Although viral gene transfer exhibits high transduction efficiency, risks such as random chromosome integration remain important challenges. Nonviral approaches are safer. Although lipofection has been used for gene transfer to various cell types *in vitro*, siRNA delivery to HSPCs is inefficient (21). Electroporation/nucleofection is efficient for delivering cargo *in vitro* (22) but is associated with low cell viability due to thermal damage from inhomogeneous electric field distribution and high current density (21–23). Synthetic nanoparticles (NPs) [e.g., based on poly(lactic-co-glycolic acid) (PLGA)] were also examined for DNA or RNA delivery *in vitro*, but with low efficiency on gene modification and gene silencing (21, 24). Better efficiency was achieved using triplex-forming peptide nucleic acid (PNA) technology (24, 25). Although 99% uptake of PLGA-NPs was demonstrated on the basis of dye fluorescence, the frequency of site-specific gene modification was less than 1% *in vitro* and even lower *in vivo*.

To overcome some of the challenges of both *in vitro* and *in vivo* cargo delivery to HSPCs, here, we demonstrate pDNA, siRNA, and miRNA delivery to HSPCs using megakaryocyte-derived MPs (MkMPs). Megakaryocytes (Mks) are large polyploidy cells derived from HSPCs upon thrombopoietin (Tpo) stimulation, which, upon maturation and fragmentation, give rise to circulating platelets (PLTs), as well as to MkMPs, which are the most abundant MPs in circulation (26). We have previously shown that, *in vitro*, Mks also shed MkMPs (27). We have also demonstrated that, *in vitro*, MkMPs specifically target and are taken up by human HSPCs through fusion and/or endocytosis following specific receptor recognition (28). MkMPs transfer cargo to HSPCs and induce potent Mk differentiation of HSPCs in the absence of Tpo, whereby RNA has been identified as a key cargo being transferred and mediating the megakaryocytic differentiation process (28). We have also shown that human MkMPs

Copyright © 2018  
The Authors, some  
rights reserved;  
exclusive licensee  
American Association  
for the Advancement  
of Science. No claim to  
original U.S. Government  
Works. Distributed  
under a Creative  
Commons Attribution  
NonCommercial  
License 4.0 (CC BY-NC).

<sup>1</sup>Department of Chemical and Biomolecular Engineering, University of Delaware, Newark, DE 19711, USA. <sup>2</sup>Delaware Biotechnology Institute, University of Delaware, Newark, DE 19711, USA. <sup>3</sup>Department of Biological Sciences, University of Delaware, Newark, DE 19711, USA.

\*Corresponding author. Email: epaps@udel.edu

can target murine HSPCs in vivo to induce de novo PLT biogenesis in a simple murine model (29), thus demonstrating in vivo target specificity and efficacy even when using a cross-species model. These findings suggest that human MkMPs may be a suitable vector system for gene and other cargo delivery to human HSPCs.

## RESULTS AND DISCUSSION

### Efficient exogenous loading of pDNA into megakaryocytic MPs through electroporation demonstrates the large cargo capacity of MPs compared to that of exosomes

Electroporation has been used as an exogenous method to load small RNAs (siRNAs or miRNAs) or small linear DNA into exosomes (10, 14–16, 30), but no reports exist for exogenous pDNA loading into MPs. Here, we developed an electroporation protocol to enable loading of pDNA to megakaryocytic MPs for delivery to HSPCs. To optimize MP loading with pDNA, we first used MPs from the model human megakaryoblastic cell line, the CHRF-288-11 cells (31). Treatment with phorbol 12-myristate 13-acetate (PMA) differentiates CHRF cells into Mks, mimicking accurately the in vitro differentiation of primary Mk cells (31), and at the same time, giving rise to MPs, here termed CMPs (CHRF-derived MPs). Nanoparticle tracking analysis (NTA; fig. S1A) shows that CMPs have an average size of 257 nm, slightly larger than the MkMP size of 234 nm. From coculture experiments of CMPs with CD34<sup>+</sup> HSPCs, similar to those using MkMPs, more than 98% of carboxyfluorescein diacetate succinimidyl ester (CFSE) dye-stained CMPs were recognized and taken up by HSPCs (fig. S1, B and C) after 30 to 60 min of coculture. Like MkMPs, CMPs program HSPCs into polyploidy Mks at day 8 of coculture (fig. S1D).

To quantify pDNA loading and delivery, we used two plasmids of different sizes and encoding an unstable and a stable green fluorescent protein (GFP). We first used the larger 6290-bp pGFPns, encoding an unstable GFP (32). pGFPns was first labeled with Cy5, and Cy5-pGFPns were loaded by electroporation at 200 V into CMPs with loading ratios (pGFPns copies per MP) of  $5 \times 10^3$ ,  $15 \times 10^3$ ,  $50 \times 10^3$ ,  $100 \times 10^3$ ,  $250 \times 10^3$ , and  $500 \times 10^3$ . The percent of Cy5<sup>+</sup> MPs from Eq. 1 (Materials and Methods) represents the efficiency of electroporation for Cy5-pGFPns loading. The number of pGFPns copies per Cy5<sup>+</sup> CMP after electroporation was calculated as described in Materials and Methods. On average, 40 to 50% of CMPs were Cy5<sup>+</sup> over a broad range of loading ratios of  $15 \times 10^3$  to  $500 \times 10^3$  (Fig. 1A). In an effort to improve the loading efficiency, we examined the impact of electroporation voltage (from 50 to 400 V) with the best loading ratio, from Fig. 1A, of  $250 \times 10^3$ . Electroporation voltage in the range examined did not affect the percent of Cy5<sup>+</sup> MPs, but higher voltage (200 and 400 V) enabled a higher loading of pGFPns per MP (Fig. 1B). Electroporation at 400 V resulted in MP aggregation and decreased the loading efficiency. To further verify pGFPns loading, CMPs loaded with pGFPns were lysed, and plasmid was extracted for a semiquantitative polymerase chain reaction (PCR) assay using a 144-bp probe on the GFP coding sequence on pGFPns (Fig. 1C). The band intensity of the amplified DNA appears proportional to the pGFPns copy number per MP (Fig. 1B), indicating successful loading of pDNA into CMPs. The faint band of the no-electroporation control corresponds to the low Cy5<sup>+</sup> fraction, and the low copy number loading of Fig. 1 (A and B) indicates that pDNA attaches to and perhaps some enter CMPs. Among the examined electroporation temperatures (25°, 37°, 45°, or 55°C), 37°C enabled the highest loading in terms of Cy5<sup>+</sup> (%) of CMPs (fig. S2), up to an average of

3455 pGFPns copies per Cy5<sup>+</sup> CMP, with a loading ratio of  $250 \times 10^3$  (Fig. 1A). These data suggest that higher membrane fluidity at the physiological temperature improves pGFPns loading. On the basis of these findings, in all subsequent studies, we used a loading ratio of  $250 \times 10^3$  pDNA copies per MP at 200 V and 37°C.

To directly visualize the loading of Cy5-labeled pGFPns into CMPs, we used super-resolution structured illumination microscopy (SIM) (33), a method not previously used for visualizing plasmid loading to EVs or cells. Before loading them through electroporation, CMPs were labeled with PKH26, a lipophilic fluorescent membrane dye. After the removal of free Cy5-pGFPns by a washing step, CMPs were added to poly-L-lysine precoated coverslips for 2 hours so that they stick to the coverslip and can be used for SIM analysis. Our CMPs have a size range of 150 to 700 nm, as determined by NTA (fig. S1A). Here, we focused on larger CMPs to enable more definitive visualization, given that Cy5 fluorescence detection requires a large number of stained plasmid molecules based on the fact that larger CMPs can carry more plasmid molecules per the discussion above. As shown in Fig. 1D, we identified several CMPs (represented by the red-stained circular membranes) with apparent sizes of 0.5 to 0.7  $\mu\text{m}$  carrying Cy5-pGFPns (cyan). We use the term apparent because acquisition of these SIM images likely overestimates the CMP size due to the nature of the SIM signal capture. To demonstrate that Cy5-pGFPns are inside the CMPs, we show a series of images of z-stack planes. As the image slice number increases, the signal from Cy5-pGFPns gradually disappears, while the CMP image (red) remains intact. These images, the first ever reported of their kind, demonstrate that Cy5-pGFPns was successfully loaded into CMPs with electroporation.

On the basis of the CMP studies, using a pDNA loading ratio of  $250 \times 10^3$ , we optimized the loading of Cy5-labeled pmaxGFP (the 3486-bp pDNA encoding a stable GFP) to MkMPs under various electroporation voltages. More than 60% of MkMPs were Cy5<sup>+</sup>, with up to an average of 4264 pmaxGFP copies per Cy5<sup>+</sup> MkMP (Fig. 1E). Both the loading efficiency from Fig. 1E and the MFI of Cy5 in Fig. 1F suggest that the best loading is obtained with 200 V. pmaxGFP loading into MkMPs was examined by PCR amplification of the cytomegalovirus (CMV) promoter using a 303-bp probe (Fig. 1G).

The plasmid loading results of Fig. 1 (A, B, and E) demonstrate the unique capability of MPs among EVs for high-capacity loading of large cargo molecules such as pDNA. It is quite remarkable that more than 3000 copies of a large 6290-bp plasmid and more than 4000 copies of the smaller 3486-bp plasmid can be loaded in these vesicles for delivery to targeted cells. How does this compare to DNA content or loading of other biological particles or vesicles? Considering the size of human mitochondria (0.5 to 3  $\mu\text{m}$ ) and mitochondria DNA (16.6 kb) (34), the copy number of loaded pDNA per MP in our study falls in the range of mitochondrial DNA copy number, which ranges from 50 to 10,000 (34). Although no quantitative data are available, Kanada *et al.* (17) demonstrated endogenous loading of pDNA into HEK293FT-derived EVs from transiently transfected donor cells, and only MPs were able to deliver functional pDNA to the recipient cells, but not exosomes.

The radius of gyration (RG) of DNA molecules (linear, open circular, or supercoil pDNA) has been used to estimate DNA loading in vesicles (35). RG represents the average distance between the mass center of DNA to each base pair. Latulippe and Zydney (35) showed that the RG of 5.76-, 9.80-, or 16.80-kb pDNA is 102, 117, or 169 nm, respectively. These results suggest that it is difficult to load large-size pDNA into nanosize exosomes (<100 nm), and are consistent with

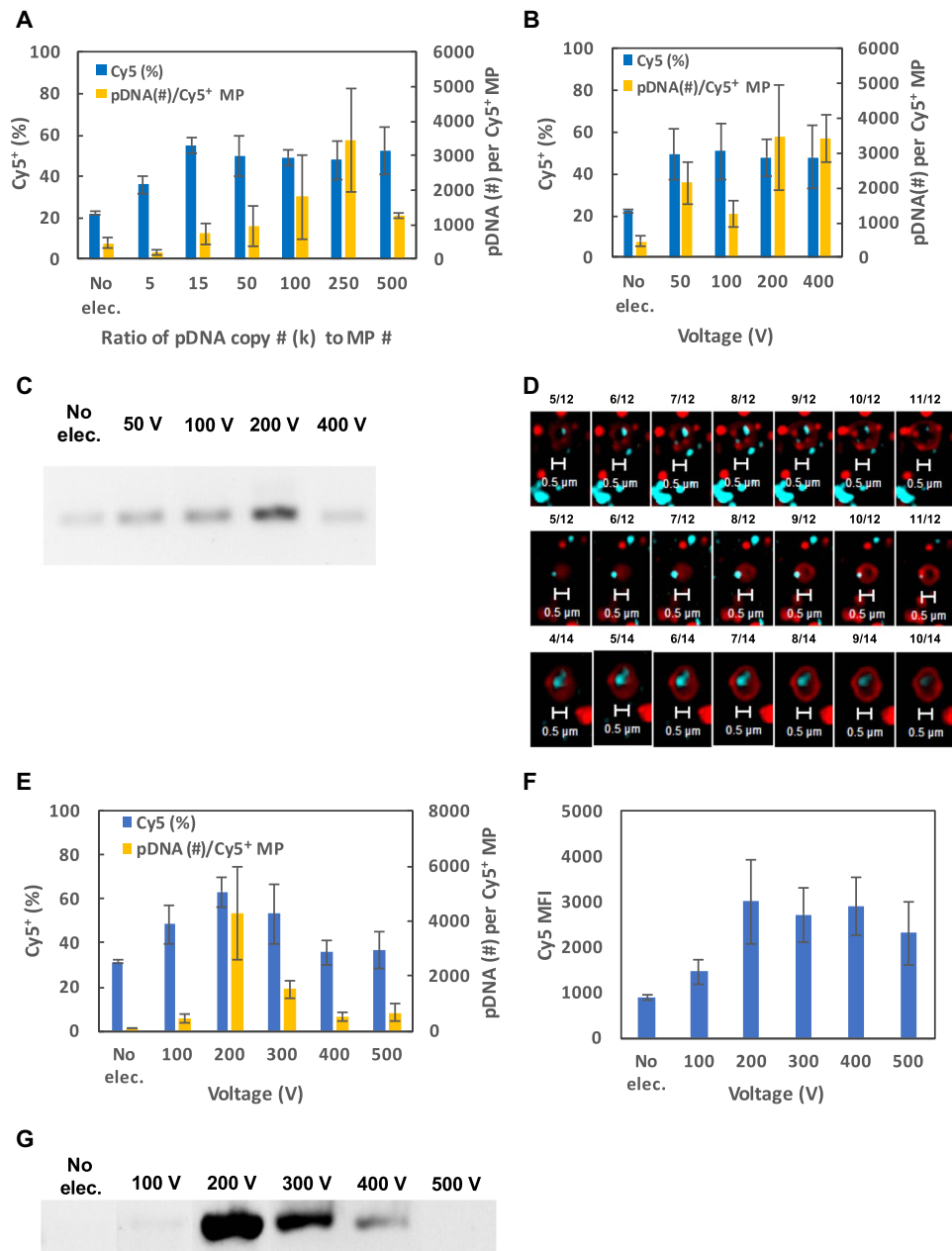


**Fig. 1. Loading of pDNA into CMPs or MkMPs through electroporation.** Loading of Cy5-labeled pGFPs was performed via electroporation under (A) different ratios of pDNA copy number to MP number and (B) different electroporation voltages. MPs were washed with phosphate-buffered saline (PBS) after electroporation. (A and B) The percent of Cy5<sup>+</sup> MPs was measured via flow cytometry. To measure the amount of loaded pDNA, MPs were lysed and pDNAs were purified for quantification to calculate the number of loaded pDNA per Cy5<sup>+</sup> MP. Loading of pGFPs into CMPs was further verified by (C) PCR amplification of a portion of the enhanced GFP (eGFP) sequence and (D) super-resolution microscopy. CMPs were first stained with PKH26 (red) for recognition. Cyan represents Cy5-pDNA. (E to G) Similarly, MkMPs were loaded with Cy5-labeled pmaxGFP via electroporation under different electroporation voltages at a pDNA/MkMP ratio of  $150 \times 10^6$ . (E) The percent of Cy5<sup>+</sup> MP, number of loaded pmaxGFP per Cy5<sup>+</sup> MP, and (F) mean fluorescence intensity (MFI) of Cy5<sup>+</sup> MPs were measured via flow cytometry. (G) Loading of pmaxGFP into MkMPs was further verified by PCR amplification of a portion of the CMV promoter sequence. Error bars in (A), (B), (E), and (F) represent SEM of three replicates.

the study of Lamichhane *et al.* (16) showing a low loading capacity of 6-kb pDNA to EVs, with an average size of about 85 nm. We estimated (table S2) that only one to two copies of the 6-kb pDNA were loaded into each 85-nm EV. A fourfold increase (about eight copies per MP) in loading capacity was obtained when using 167-nm MPs (table S2) (16). On the basis of these findings, the larger size (257 nm) of CMPs or MkMPs (234 nm) in our study would be able to accom-

modate an even larger number of plasmid copies. However, our data far exceed what one would expect from any extrapolation of the data of the Latulippe and Zydny (35) study: Loading an average of more than 3400 copies of a 6290-bp plasmid per CMP (Fig. 1, A and B) or more than 4200 copies of a 3486-bp plasmid per MkMP (Fig. 1E) is more than two orders of magnitude higher and represents the highest DNA loading ever reported for EVs, thus demonstrating the

potential of using MPs for delivering large amounts of cargo to desirable cell targets. We also estimated the capacity of our megakaryocytic MPs for loading larger pDNAs on the upper size range of what has been used for gene delivery, such as the supercoiled 9.8-kb plasmid reported by Latulippe and Zydney (35). The RG of this pDNA is 117 nm, which is 14.7% larger in radius or 50.9% larger in occupied volume than a 5.76-kb supercoiled pDNA (RG = 102 nm). Together with our results (3455 or 4264 copies per MP; Fig. 1), we estimate that the copy number of the 9.8-kb pDNA per MP will be ca. 51% smaller, or about 1700 to 2100 copies per MP (table S2). This is still a large plasmid loading capacity and more than sufficient for functional plasmid delivery to HSPCs.

### Delivery of pDNA to HSPCs using CMPs or MkMPs

CMPs were loaded with pGFPns using the optimized electroporation protocol. After electroporation, large particle aggregates due to elec-

trapolation were separated from regular-size MPs by centrifugation (Fig. 2A). Cy5-pGFPns-loaded MPs were washed once with PBS and cocultured with day 1 HSPCs for up to 72 hours. Delivery of pGFPns was first confirmed through the isolation of pDNA from HSPCs harvested after 24 hours of coculture. The eGFP-encoding DNA sequence was probed by semiquantitative PCR and detected only from coculture samples with pGFPns-loaded CMPs (Fig. 2B). We hypothesized that the gravity- or centrifugation-driven medium flow-through (FT) commercial Transwell system would enhance the physical interaction between CMPs and HSPCs. Thus, we carried out cocultures under four different settings/conditions: (i) HSPC/CMP coculture in Eppendorf tubes in a small volume for 1 hour and transferred to standard 24-well plates; (ii) HSPCs/CMPs seeded onto the membrane inserts of 24-well Transwell plates (Fig. 2C, FT system); (iii) coculture in the FT system as above, but with enhanced medium flow using 600g centrifugation of the plates for 30 min to further

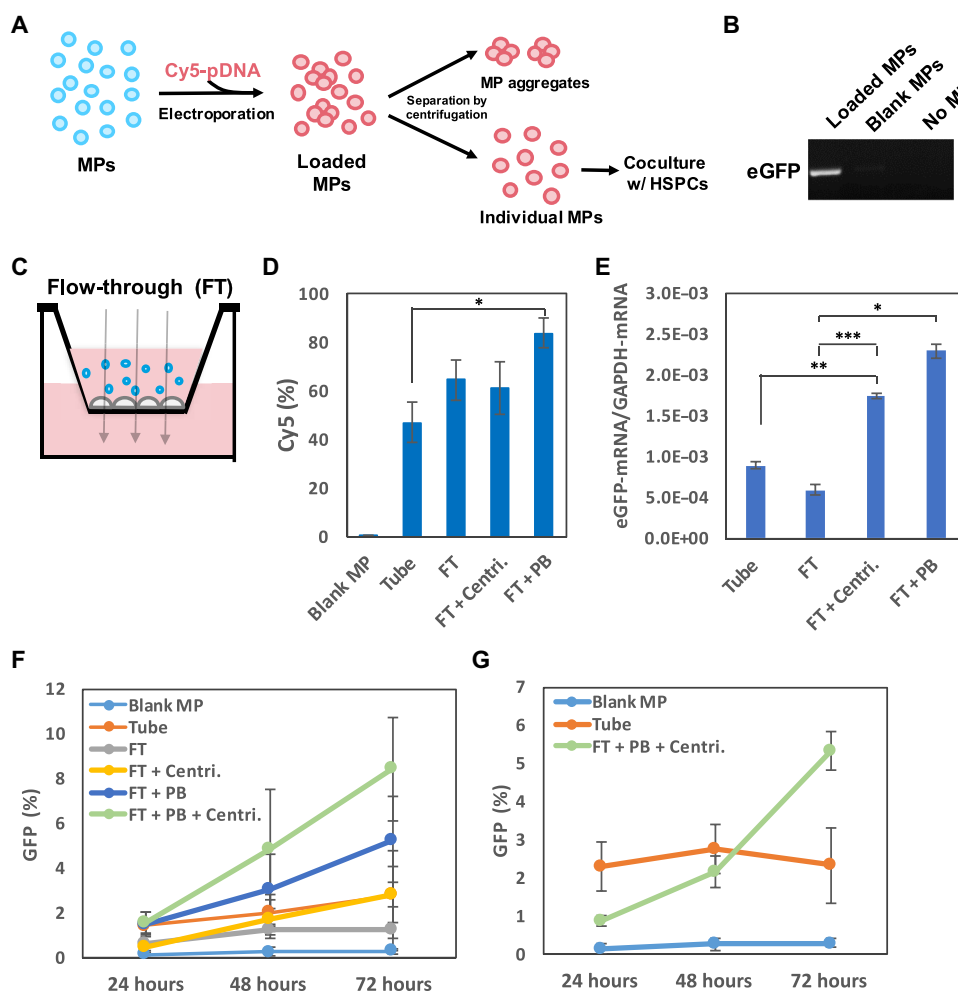


**Fig. 2. Delivery of pDNA to HSPCs via MPs.** (A) Schematic showing the separation of aggregates from individual MPs after loading of pDNA via electroporation. (B) Loading of pGFPns was confirmed in day 1 cells from the coculture of HSPCs with pGFPns-loaded CMPs via PCR amplification of a portion of the eGFP sequence. (C) Schematic of FT setup with 0.4-μm membrane insert. HSPCs were first seeded onto the membrane for 30 min, and MPs were then added to the culture. (D and E) Day 1 HSPCs were cocultured with Cy5-pGFPns-loaded MPs in Eppendorf tubes (Tube), the FT system (FT), the FT system with centrifugation (FT + Centri.), or the FT system but with medium supplemented with PB (8 μg/ml) (FT + PB). Cells were harvested for (D) flow cytometric analysis of Cy5 signal at 24 hours and (E) eGFP-mRNA and GAPDH-mRNA quantification by qRT-PCR at 72 hours. (F and G) Day 1 HSPCs were cocultured with pmaxGFP-loaded (F) CMPs or (G) MkMPs under five coculture conditions (Tube, FT, FT + Centri., FT + PB, and FT + PB + Centri.). Cells were harvested at 24, 48, and 72 hours for measuring GFP expression by flow cytometry. Native MPs were used as control (Blank MP). Data in (D) and (E) represent averages of three biological replicates ± SEM. \* $P < 0.05$ , \*\* $P < 0.01$ , and \*\*\* $P < 0.001$ .

enhance the physical contact between the HSPCs and CMPs; and (iv) coculture in the FT system with supplementation of polybrene (PB; 8  $\mu\text{g}/\text{ml}$ ). The polycation PB (36) was used to test if it would enhance the interaction between HSPCs and CMPs. After 24 hours of coculture, the percent of  $\text{Cy}5^+$  HSPCs was measured by flow cytometry. Forty-seven percent of HSPCs were  $\text{Cy}5^+$  from the coculture in Eppendorf tubes, while 65% of HSPCs were  $\text{Cy}5^+$  in the FT system without centrifugation (Fig. 2D). Centrifugation did not affect the percent of  $\text{Cy}5^+$  HSPCs, but PB additions promoted CMP uptake to obtain 84% of detectable  $\text{Cy}5^+$  HSPCs (Fig. 2D and fig. S3A).

Next, we examined the functionality at the transcriptional level of the delivered pGFPns. Total RNA was isolated from each coculture at 72 hours, and eGFP-mRNA expression was examined by quantitative reverse transcription PCR (qRT-PCR). Figure 2E shows the expression ratio of eGFP-mRNA to the reference gene glyceraldehyde-3-phosphate dehydrogenase (GAPDH)-mRNA. Both centrifugation and PB addition increased the level of eGFP-mRNA by 2.93- and 3.86-fold, respectively. Unexpectedly, there was no significant difference in eGFP expression between the two simpler settings (tube and FT without centrifugation). On the basis of these results, we hypothesize that the combination of physical and chemical enhancement will give rise to better functional pDNA delivery. To test that, we investigated the GFP expression at the translation level. We examined the GFP expression from both plasmids. We first show data using pmaxGFP. In addition to four coculture methods described above, HSPCs were cocultured with pmaxGFP-loaded CMPs or MkMPs in the FT system with supplementation of PB (8  $\mu\text{g}/\text{ml}$ ) and with 600g centrifugation of the plates for 30 min (FT + PB + Centri.). The percent of  $\text{GFP}^+$  HSPCs was measured at 24, 48, and 72 hours of coculture by flow cytometry. The results (Fig. 2, F and G, and fig. S3B) show that centrifugation with PB addition promotes functional delivery of pmaxGFP, with more than 8 or 5% of cells expressing GFP with the delivery by CMPs or MkMPs, respectively. These data show that our system delivers pDNA to the nucleus.

We used SIM to directly visualize pGFPns delivery and cellular localization, as well as eGFP expression. Cells cocultured with pGFPns-loaded CMPs (we used the less stable GFP to potentially capture the dynamics of delivery) were prestained with DiI, a lipophilic dye for cellular membrane staining, while pGFPns was prelabeled with Cy5. At 24 hours [which corresponds to 0.8 cell doublings (37)], cyan-identified  $\text{Cy}5$ -stained pGFPns were concentrated at both the cellular membranes (red staining) and the nuclear [4',6-diamidino-2-phenylindole (DAPI) staining] areas, but no eGFP expression was detectable (Fig. 3). At 72 hours, which corresponds to 2.4 cell doublings, pGFPns persists on the cytoplasmic membrane but is not visible in the nucleus. This is likely the result of the reduced stability of the GFP encoded on this plasmid. However, eGFP expression is widespread in the two cells shown and is apparently concentrated near intracellular, red-stained membranes, likely corresponding to membranes of the rough endoplasmic reticulum (ER) and various Golgi organelles. These SIM data further support the successful delivery of pGFPns to the HSPC nucleus and capture some of the dynamics of the process: plasmid delivery to the nucleus followed by protein expression in cytoplasmic organelles. This is the first report of direct visualization via SIM of pDNA delivery to the nucleus and the associated detailed localization of protein expression.

### Effective delivery of pDNA to HSPC nuclei

Although up to 84% of cells cocultured with  $\text{Cy}5$ -pDNA-loaded MPs were  $\text{Cy}5^+$  (Fig. 2D), only up to 10% of cells were expressing GFP

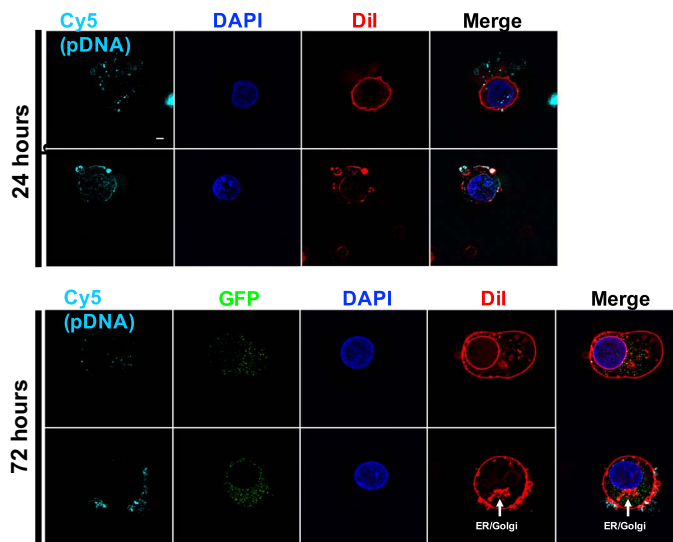


**Fig. 3. HSPCs cocultured with  $\text{Cy}5$ -pGFPns-loaded MPs were harvested and fixed at 24 and 72 hours.** The location of  $\text{Cy}5$ -pGFPns (cyan) and eGFP expression (green) were examined by super-resolution microscopy. Nucleus was stained with DAPI (blue), and cellular membrane was stained with DiI (red).

(Fig. 2F), suggesting that flow cytometric analysis may not be capturing all the GFP-expressing cells due to detection limitations deriving from lower levels of GFP expression. We thus directly examined the effectiveness of pDNA delivery to nuclei. Briefly, HSPCs were cocultured with  $\text{Cy}5$ -pmaxGFP-loaded CMPs or MkMPs under various conditions as before. After 24 hours, nuclei were isolated and analyzed via flow cytometry. As shown in Fig. 4 (A and B), up to 81 or 75% of HSPC nuclei were  $\text{Cy}5^+$ , which is a considerably higher fraction than for direct plasmid electroporation, indicating the effective delivery of pmaxGFP to the nuclei using either CMPs or MkMPs. Notably, addition of PB enhanced both the percent of  $\text{Cy}5^+$  nuclei and their MFI by up to twofold (Fig. 4, C and D), suggesting its role in improving pDNA transport to nucleus. This high percentage (75 to 81%) of delivery to nuclei was unexpected given that plasmid delivery via electroporation results in higher GFP expression ( $54.1 \pm 2.4\%$ ). This is likely due to the different mechanisms of pDNA delivery to cell nuclei. Plasmid delivery by electroporation (known as nucleofection) is a quick process delivering pDNA to the nucleus by opening pores to the nuclear envelope without the need for cell cycling, which is otherwise necessary for pDNA entry into the nucleus (38, 39). Thus, with pDNA nucleofection, protein expression starts within 3 to 6 hours, and because of cell cycling, a fraction of the plasmid is diluted or degraded within 24 hours, thus resulting in a lower percentage of  $\text{Cy}5^+$  nuclei. In contrast, delivery of pDNA through MPs requires cell cycling and mitosis, which are necessary for breaking down the nuclear envelope to enable pDNA entry into the nucleus (39). We should note also that direct comparison in terms of GFP expression between electroporation/ nucleofection may induce nonspecific changes in cell metabolism and may alter the subcellular protein expression patterns of the transgene (40). Together, these data show that MkMPs can effectively deliver pDNA to HSPCs and HSPC nuclei. Nevertheless, to achieve better protein expression, delivery of pDNA to the nucleus can be further increased by (i) increasing the ratio of MkMPs per HSPC to 50 to 150 so that more pDNA is delivered to HSPC and HSPC nuclei; (ii) using

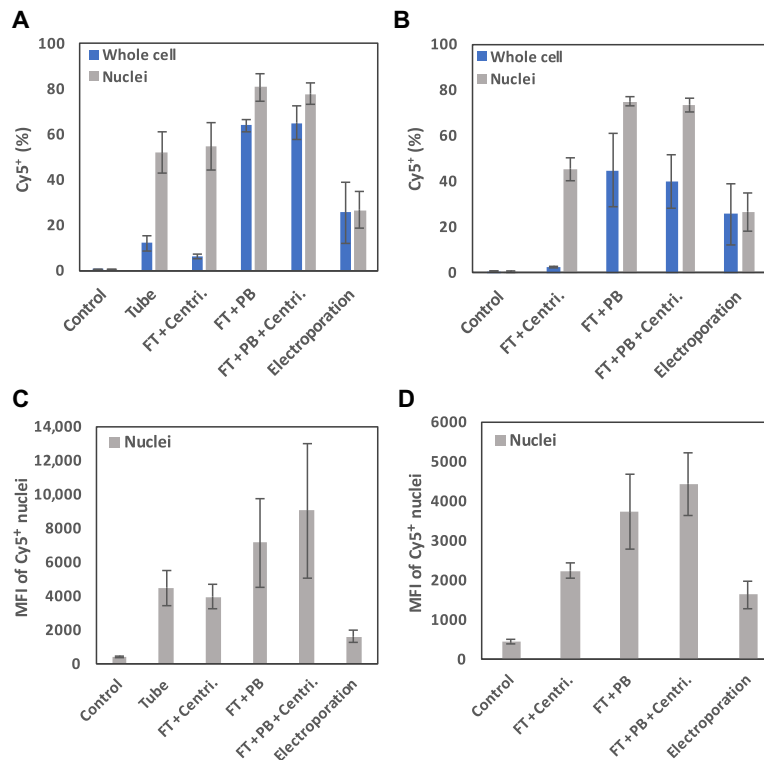


**Fig. 4. Examining the delivery of pDNA to HSPC nucleus via nuclei analysis.** Day 1 HSPCs were cocultured with Cy5-pmaxGFP-loaded (A and C) CMPs or (B and D) MkMPs in Eppendorf tube (Tube), FT system with centrifugation (FT + Centri.), FT supplemented with PB (8  $\mu$ g/ml) (FT + PB), or the combination of PB with centrifugation in FT system (FT + PB + Centri.). Both cells and isolated nuclei were harvested for flow cytometric analysis on (A and B) Cy5<sup>+</sup> nuclei percentage or (C and D) MFI of Cy5<sup>+</sup> nuclei at 24 hours. Data represent averages of three biological replicates  $\pm$  SEM.

cationic polymers such as polyethylenimine, which has been shown to enhance endosomal escape (41, 42); or (iii) using pDNA complexed with nuclear localization signal peptides such as the SV40 antigen, which can enhance plasmid nuclear import (43, 44).

#### Functional synthetic RNA delivery to HSPCs using MkMPs

Beyond pDNA delivery, small RNAs (miRNAs or siRNAs) constitute an important cargo for a broad variety of therapeutic applications, especially so for delivery to HSPCs (20–22). We have shown that the RNA content of MkMPs is responsible for megakaryocytic differentiation and PLT biogenesis of the targeted HSPCs (27, 28), thus showing that RNA delivery to HSPCs is an effective process. We have also discussed that transfusion of human MkMPs in mice leads to de novo murine PLT biogenesis (29), thus showing that in vivo RNA delivery to HSPCs is effective in enabling the development of a complex biological phenotype. Here, we examined the delivery of synthetic RNAs, namely, an siRNA and an miRNA, to HSPCs through MkMPs. While the ultimate goal is in vivo delivery, here, we examined in vitro delivery as the first step to assess the efficacy of the process, assuming that in vivo delivery will be efficacious, as our murine experiments suggest.

We modified the electroporation protocol we used for pDNA loading to CMPs to load siRNA to MkMPs to deliver to and silence *c-myb* expression in HSPCs. *c-myb* is a major regulator of erythropoiesis and megakaryopoiesis by restraining megakaryopoiesis at the common erythroid-megakaryocytic progenitor stage through a mechanism involving miR-486-3p (45, 46). Bianchi *et al.* (45) silenced *c-myb* expression using siRNA (delivered directly through electro-

poration) to enhance Mk differentiation of CD34<sup>+</sup> HSPCs. To assess the effectiveness of siRNA delivery through MkMPs, we first loaded Alexa 647-labeled siRNA (nonspecific targeting siRNA) to MkMPs by electroporation and examined the level of the loading effectiveness by flow cytometric analysis. We found that  $24.3 \pm 9.0\%$  of MkMPs were Alexa 647<sup>+</sup>. To assess the ability of siRNA-loaded MkMPs to deliver siRNA to HSPCs, we used cocultures of MkMPs with cultured day 1 HSPCs. Thirty-five percent of the cells were Alexa 647<sup>+</sup> after 48 hours of coculture, showing stable Alexa 647 staining up to 120 hours of coculture, thus demonstrating effective delivery of siRNA to HSPCs (Fig. 5A). On the basis of these findings, we next examined functional siRNA delivery to HSPCs. We assessed the enhancing impact of siRNA targeting *c-myb* (siR-MYB) via MkMP delivery, beyond the impact of the siRNA negative control (siR-Neg) or that of native MkMPs, which promote Mk differentiation of HSPCs by several mechanisms, apparently including MYB down-regulation as shown below. Briefly, siRNA-loaded MkMPs or control MkMPs were cocultured with HSPCs, and cells were analyzed by flow cytometry for CD41 (Mk marker) or CD34 expression at days 3, 5, and 8. Delivery of siR-MYB via MkMPs increased the percentage of CD41<sup>+</sup> and CD34<sup>+</sup> CD41<sup>+</sup> cells by up to 21 and 19%, respectively, at day 8 of coculture versus controls (MkMP-siR-Neg or native MkMPs) (Fig. 5, B and C). These data suggest the functional delivery of siR-MYB to HSPCs through MkMPs. Silencing of *c-myb* was also confirmed by qRT-PCR at day 1 of coculture (Fig. 5D). MYB expression decreased by 27% from the impact of cargo contained in unmodified MkMPs versus vehicle control and by 33% from the delivery of MkMPs loaded with siR-MYB, indicating the silencing of *c-myb* through siR-MYB.

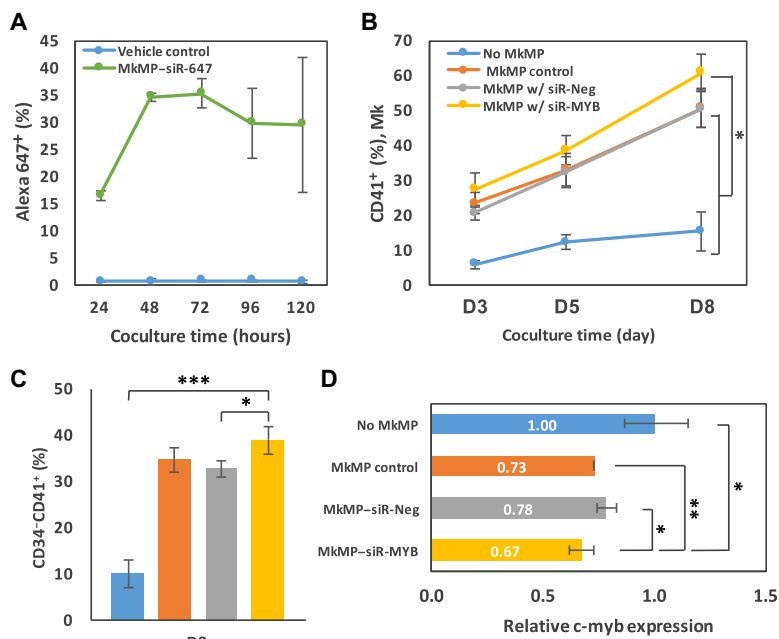


**Fig. 5. Silencing of *c-myb* through MkMP delivery of siRNA to HSPCs enhanced megakaryocytic differentiation.** MkMPs were loaded with Alexa 647-labeled siRNA (green), siRNA negative control (siR-Neg, gray), or siRNA targeting MYB (siR-MYB, yellow) by electroporation. HSPCs were cocultured with siRNA-loaded MkMPs, MkMPs without any siRNA (MkMP control, orange), or without MkMPs (No MkMP, blue). (A) Delivery efficiency of siRNA to HSPC via MkMPs was examined on the basis of Alexa 647<sup>+</sup> percentage of cells by flow cytometric analysis. (B and C) Cells from each coculture were harvested for flow cytometric analysis on CD41<sup>+</sup> (%) at days 3, 5, and 8 and on CD34<sup>+</sup>CD41<sup>+</sup> (%) at day 8. (D) Level of *c-myb* was quantified by qRT-PCR from each coculture at 24 hours, normalized to the expression of *GAPDH* as a reference gene. Data in (B) to (D) represent averages of three biological replicates ± SEM. \**P* < 0.05, \*\**P* < 0.01, and \*\*\**P* < 0.001.

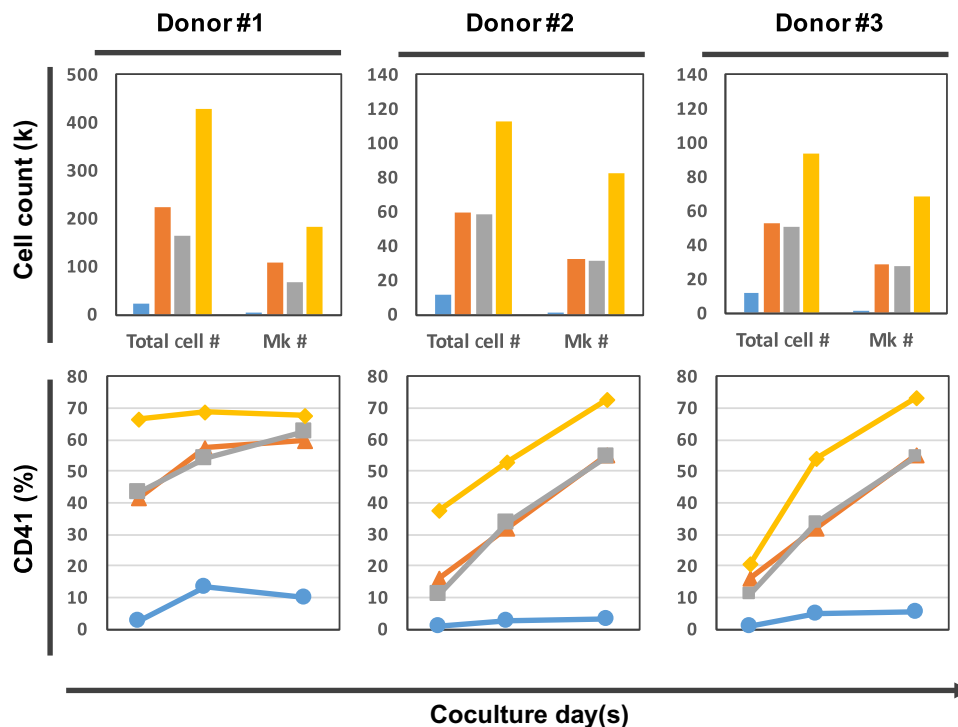


**Fig. 6. Functional delivery of miR-486-5P to HSPCs via MkMPs enhanced megakaryocytic differentiation.** MkMPs were loaded with 8 μM miR-NC or miR-486-5P mimics by electroporation. CD34<sup>+</sup> HSPCs (60,000) were cocultured with vehicle control (blue, circle), MkMP control (orange, triangle), miR-NC-loaded MkMPs (gray, square), or miR-486-5P-loaded MkMPs (gold, diamond) for up to 8 days. (Top) A number of total cells or Mks were counted at day 8 of coculture. (Bottom) CD41 (Mk marker) expression was examined at days 3, 5, and 8 of coculture by flow cytometric analysis. Three biological replicates of coculture are shown.

These functional changes brought about by the delivery of siR-MYB are typical effects observed with most siRNAs, especially in the background of these MPs, which promote Mk differentiation.

Next, we examined the functional delivery of miR-486-5p. miR-486-5p has been shown to play an important role in regulating the proliferation, survival, and differentiation of CD34<sup>+</sup> cells. Notably, it is expressed in megakaryocytic-erythroid progenitors and regulates their proliferation and survival by regulating AKT signaling and the transcription factor FOXO1 (47). We thus hypothesized that miR-486-5p delivery will promote cell proliferation and megakaryocytic-erythroid differentiation and expansion. We loaded a miR-486-5p double-stranded mimic RNA or miR-NC (nontargeting miRNA negative control) to MkMPs via electroporation. Unmodified MkMPs or miRNA-loaded MkMPs were cocultured with CD34<sup>+</sup> HSPCs for 8 days. Because of natural response variations of CD34<sup>+</sup> cells from different donors, the data from three coculture biological replicates are presented individually in Fig. 6. At day 8 of coculture, miR-486-5p delivered by MkMPs significantly increased total cell numbers and Mk numbers (CD41<sup>+</sup> cells) by up to 91 and 169%, respectively, compared to the coculture of miR-NC-loaded MkMPs or unmodified MkMPs with HSPCs. Although CD41 expression varied at early culture (day 3) with different donor CD34<sup>+</sup> cells, it reached similar levels at day 8 for all three donor cells. Compared to native MkMPs or miR-NC-loaded MkMPs, miR-486-5p delivery enhanced the fraction of CD41<sup>+</sup> by 10 to 20%.

HSPCs are hard-to-transfect primary stem cells (19). Among studies using synthetic nanoparticles (NPs), only one NP form has demonstrated the ability to deliver cargo to HSPCs (24, 25). McNeer *et al.* (24) demonstrated delivery to HSPCs using biodegradable PLGA-NPs loaded with triplex-forming PNAs and single-stranded donor DNA. Although presenting a great advance, the gene modification efficiency was less than 1% *in vitro* (24) and even lower *in vivo* (25). In our study, for the first time, we successfully demonstrated the delivery of pDNA for functional protein expression and of small RNAs (miRNA and siRNA) for gene regulation/silencing in HSPCs using megakaryocytic MPs. Our study supports the potential of MkMPs for applications in gene and cell therapy targeting HSPCs. Our data also support the use of the larger MPs for delivering larger amounts and larger-size cargo to target cells.

## MATERIALS AND METHODS

### Experimental design

On the basis of our previous studies on the role and characterization of megakaryocytic MPs, and their ability to specifically target and deliver their cargo to HSPCs (27, 28), the aim of this study was to develop a system to deliver pDNA and small RNAs to HSPCs using human MkMPs. We examined functional delivery of pDNA using labeled pDNA and GFP protein expression. We also evaluated the delivery of two types of small RNA, siRNA and miRNA, using functional assays. All experiments were carried out with at least three biological and multiple technical replicates for statistical significance.

### Chemicals and reagents

Recombinant human interleukin-3 (IL-3), IL-6, IL-9, IL-11, stem cell factor (SCF), and Tpo were purchased from PeproTech Inc. BIT 9500 was purchased from STEMCELL Technologies. Anti-CD61 magnetic microbeads and MACS cell separation tools were purchased from Miltenyi. Fluorescein isothiocyanate (FITC)-conjugated anti-CD41,

allophycocyanin (APC)-conjugated anti-CD34, and immunoglobulin G antibodies were purchased from BD Biosciences. Anti-GFP (ab290) and corresponding isotype control (ab171870) antibodies were from Abcam. siR-MYB, siR-negative control, miR-486-5p mimics, miR-negative control, CellTracker CM-DiI Dye, and SlowFade Diamond Antifade Mountant with DAPI were purchased from Thermo Fisher Scientific. Alexa 647-conjugated AllStars Negative Control siRNA and the miRNeasy Micro Kit were purchased from Qiagen. All other chemicals were purchased from Sigma-Aldrich.

### Cultures of HSPCs and CHRF cells

Frozen G-CSF (granulocyte colony-stimulating factor)-mobilized human peripheral blood CD34<sup>+</sup> cells were obtained from Fred Hutchinson Cancer Research Center. Megakaryocytic cultures were set up as described (37). Briefly, CD34<sup>+</sup> cells were cultured in Iscove's modified Dulbecco's medium (IMDM; Gibco) supplemented with 20% BIT 9500 (STEMCELL Technologies), Tpo (100 ng/ml), SCF (100 ng/ml), IL-3 (2.5 ng/ml), IL-6 (10 ng/ml), IL-11 (10 ng/ml), and human low-density lipoprotein under 5% O<sub>2</sub> for 5 days. From days 5 to 7, IL-3 was increased to 10 ng/ml and IL-6 was substituted with IL-9 (10 ng/ml). At day 7, CD61<sup>+</sup> cells (Mks) were enriched by anti-CD61 magnetic microbeads (Miltenyi) using MACS separation (Miltenyi). MkMPs were isolated from culture medium from day 12 Mk culture

CHRF cells (31) were cultured in growth medium [IMDM supplemented with 10% fetal bovine serum (Sigma-Aldrich)] for 3 days to reach the concentration at 500,000 to 1,000,000 cells/ml. Cells were then treated with PMA (10 ng/ml) and reseeded at 200,000 cells/ml in fresh medium. CMPs were isolated from culture medium at day 4 after PMA treatment.

### Isolation of MkMPs and MPs (CMPs) from CHRF cells

MkMPs or CMPs were isolated as described (27, 28). Briefly, cells and cell debris were removed from the culture medium by centrifugation at 2000g for 10 min. MPs were then enriched via ultracentrifugation (Optima Max Ultracentrifuge and Rotor TLA55, Beckman Coulter) under 25,000 rpm for 30 min at 4°C. After that, MPs were resuspended in PBS or stored at -80°C until used.

### Determination of MP size distribution

MkMPs or CMPs resuspended in PBS were first diluted 140-fold in deionized water. Their size distribution was measured by NTA using NanoSight NS300 (Malvern). Each analysis was carried out with five measurements, with the camera level set at 9 to 10, the detection threshold at 4, and 50 to 80 particles per frame with 1500 frames per measurement.

### Exogenous loading of pDNA to CMPs or MkMPs

The 6290-bp reporter plasmid pGFPns was a gift of H. Gu (Addgene plasmid #35626) (32). The 3486-bp pmaxGFP was part of the Amara Nucleofection Kit (Lonza). pGFPns or pmaxGFP was first conjugated with Cy5 by Label IT Tracker Cy5 (Mirus), following the manufacturer's protocol, with labeling density of 4 to 10 label molecules per plasmid molecule. CMPs were isolated from day 4 cultured CHRF cells, and MkMPs were purified from day 12 CD34<sup>+</sup> cell-derived Mk culture. After washing once with 1 ml of PBS by ultracentrifugation at 25,000 rpm for 30 min at 4°C, MPs were resuspended in hypotonic buffer (Eppendorf). CMPs ( $5 \times 10^6$ ) were then mixed with Cy5-labeled pGFPns at various pGFPns/CMP ratios ( $5 \times 10^3$ ,  $15 \times 10^3$ ,

$50 \times 10^3$ ,  $100 \times 10^3$ ,  $250 \times 10^3$ , or  $500 \times 10^3$ ) in a total volume of 100  $\mu$ l and incubated for 15 min at 37°C. pGFPns was loaded into CMPs by electroporation (Gene Pulser Xcell Electroporation System, Bio-Rad) using an exponential decay pulse for 10 to 20 ms at 100  $\mu$ F, 37°C in a 2-mm cuvette. Following that, 900  $\mu$ l of wash buffer (IMDM + 2% BIT + 2 mM EDTA) was added to ameliorate nucleic acid or MP aggregation, and loaded MPs were incubated on ice for 20 min for recovery, followed by centrifugation at 1000g for 10 min to remove large aggregates generated due to electroporation. Loaded MPs were collected and washed once with PBS under ultracentrifugation at 25,000 rpm, 4°C for 30 min and resuspended in PBS or coculture medium.

### Exogenous loading of small RNAs to MkMPs

MkMPs ( $4 \times 10^6$  to  $5 \times 10^6$ ) were loaded with siRNA targeting *c-myb* (siR-MYB, Ambion) or Alexa 647–conjugated AllStars Negative Control siRNA (Qiagen) by electroporation in a 4  $\mu$ M siRNA solution at 150 V, 100  $\mu$ F in a 4-mm cuvette at 4°C. Similarly,  $4 \times 10^6$  to  $5 \times 10^6$  MkMPs were loaded with miR-486-5P mimic (8  $\mu$ M solution) or miR-NC by electroporation at 150 V, 100  $\mu$ F in a 2-mm cuvette at 4°C. After loaded MkMPs were recovered in wash buffer at 4°C for 30 min, large aggregates were isolated under 1000g for 10 min, while small loaded MkMPs were washed twice with PBS under ultracentrifugation at 25,000 rpm at 4°C for 30 min and resuspended in IMDM for coculture experiments.

### Quantification of plasmid-DNA loading of CMPs or MkMPs

Quantified by flow cytometry,  $Cy5^+$  (%) of MP population (Eq. 1) represents the  $Cy5$ -pDNA loading efficiency

$$\text{Loading efficiency (\%)} = \frac{Cy5^+MP\#}{\text{TotalMP}\#} \quad (1)$$

pDNA (pGFPns or pmaxGFP) was purified from loaded MPs using the QIAprep Spin Miniprep Kit (Qiagen), and its concentration was quantified using the Qubit dsDNA HS Assay Kit (Invitrogen). To calculate the pDNA copy number per  $Cy5^+$  MPs, we calculated the molecular mass (M.M.) of pDNA (6290 bp of pGFPns or 3486 bp of pmaxGFP), which is  $3.9 \times 10^6$  or  $2.1 \times 10^6$  g/mol, respectively. On the basis of the pDNA concentration quantified from Qubit, the total number of pDNA copies is calculated using Eq. 2, where  $N_A$  is the Avogadro number

$$\text{pDNA copy\#} = \frac{\text{Loaded pDNA (ng)} * 10^9}{\text{M.M.}} \times N_A \quad (2)$$

The pDNA copy number per  $Cy5^+$  MP was calculated on the basis of the number of  $Cy5^+$  MPs. pGFPns purified from loaded CMPs was confirmed through PCR amplification of the GFP sequence using a 144-bp probe, while pmaxGFP was confirmed by targeting the CMV promoter sequence using a 303-bp probe. Primers for PCR amplification are listed in table S1. PCR amplicons were visualized by gel electrophoresis.

### Setup of cocultures of HSPCs with pDNA-loaded CMPs/MkMPs or small RNA–loaded MkMPs

Cocultures of MPs with  $CD34^+$  cells were set up as described (27, 28). Briefly, for pDNA delivery, 60,000 HSPCs from day 1 of culture were cocultured with  $Cy5$ -pmaxGFP–loaded CMPs or MkMPs with a ratio of 150 CMPs per cell or 20 MkMPs per cell under five different

conditions: (i) (Tube) HSPCs and MPs were first cocultured in a small volume (50 to 100  $\mu$ l) in Eppendorf tubes and diluted in 1-ml coculture medium in 24-well plate (27, 28). (ii) (FT) HSPCs were first seeded onto the upper compartment of the Transwell insert (0.4- $\mu$ m pore size; Corning). After 30 min, MPs were added into the culture. (iii) (FT + Centri.) HSPC-MP coculture was set up as in (ii) above in the FT system in a 24-well plate. After adding the MPs, the plate was centrifuged under 600g for 30 min at room temperature to physically enhance the contact between HSPCs and MPs. (iv) (FT + PB) HSPCs were pretreated with PB (8  $\mu$ g/ml) for 15 min at 37°C, followed by coculture with MPs in the FT system as in (ii). (v) (FT + PB + Centri.) HSPCs were pretreated with PB (8  $\mu$ g/ml) for 15 min at 37°C, followed by coculture with MPs in the FT system with the centrifugation under 600g for 30 min at room temperature, as the combination of (iii) and (iv). The percent of  $Cy5^+$  cells at 24 hours and GFP expression at 24, 48, and 72 hours of each coculture were determined by flow cytometry.

For siRNA or miRNA delivery, 60,000 of HSPCs from day 1 of culture were cocultured with MkMPs loaded with siR–Alexa 647, siR–MYB, siR–NC (nontargeting siRNA negative control), miR–486-5p mimic, and miR–NC (nontargeting miR–NC); unloaded MkMPs at a ratio of 30 MkMPs per cell; or without MkMPs as vehicle control in IMDM supplemented with 10% BIT 9500, SCF (50 ng/ml), and 1 $\times$  antibiotic-antimycotic at 37°C and 20%  $O_2$  for up to 8 days. An additional dose of Tpo (10 pg/ml) was added in the siRNA delivery experiment. This minimal amount of Tpo was used to induce *c-myb* expression so that its down-regulation via siR–MYB can be observed. Cells from the coculture with siR–Alexa 647–loaded MkMPs were harvested at days 1 to 5 for flow cytometric analysis to measure the percent of Alexa 647 $^+$  cells. At days 3, 5, and 8, cells cocultured with siR–MYB, siR–NC–loaded MkMPs, or unloaded MkMPs were stained with FITC-conjugated anti-CD41 and APC-conjugated anti-CD34 antibodies for flow cytometric analysis of CD41 and CD34 expression. In miRNA delivery experiment, cells cocultured with MkMPs loaded with miR–486-5p, miR–NC, or unloaded MkMPs were harvested at days 3, 5, and 8 for flow cytometric analysis on CD41 expression. The total cell count and Mk count were calculated at day 8.

### Quantitative reverse transcription polymerase chain reaction

To evaluate the delivery of pDNA, at 24 hours, cells cocultured with pGFPns-loaded CMPs were first washed with PBS, and pGFPns from cells was purified using the QIAprep Spin Miniprep Kit. A probe for the eGFP sequence was amplified through PCR, as detailed above, to confirm the delivery of pGFPns to HSPCs. At 72 hours, total RNA was isolated from the cells using the miRNeasy Micro Kit (Qiagen), and 0.5  $\mu$ g of total RNA was reverse transcribed by the cDNA Reverse Transcription Kit (Applied Biosystems). qRT-PCR assays for *eGFP* and *GAPDH* mRNA expression were performed with iTaq Universal SYBR Green Supermix (Bio-Rad). *eGFP* and *GAPDH* expression was quantified by the Livak method. To verify the level of gene knockdown of *c-myb* expression, total RNA was isolated at day 1 of coculture, and qRT-PCR analysis was performed with iTaq Universal SYBR Green Supermix. The gene expression level of *c-myb* was calculated with normalization to *GAPDH*. Primers used for qRT-PCR are listed in table S1

### Super-resolution microscopy

To visualize the delivery of pGFPns to HSPCs, at 24 and 72 hours, HSPCs from the coculture with  $Cy5$ -pGFPns were examined by

ELYRA PS.1 Superresolution Microscopy (Zeiss). Briefly, cells were first stained with CellTracker CM-DiI Dye (Invitrogen) for lipid membrane staining and seeded onto poly-L-lysine-coated coverslips. After 10 min, cells were fixed with 4% paraformaldehyde for 10 min at room temperature. After washing with PBS thrice, samples were mounted with SlowFade Diamond Antifade Mountant with DAPI (Invitrogen) for imaging.

### Nuclei isolation

HSPCs (60,000) from day 1 of culture were cocultured with Cy5-pmaxGFP-loaded CMPs or MkMPs with a ratio of 50 CMPs per cell or 20 MkMPs per cell under four different conditions as described above (Tube, FT + Centri., FT + PB, and FT + PB + Centri.). Isolation of nuclei was performed at 24 hours of coculture, following the Nabbi and Riabowol's protocol (48). Briefly, cells were collected from each coculture, washed twice with ice-cold PBS, and pelleted at 500g for 4 min. After removing the supernatant, the pellet was first resuspended in 100  $\mu$ l of ice-cold PBS and lysed in 900  $\mu$ l of ice-cold PBS containing 0.1% NP-40. The sample was then pipetted five times, followed by centrifugation at 10,000 rpm for 10 s to collect the nuclei fraction. The supernatant containing cytoplasmic fraction was removed, and the nuclei pellet was washed again with ice-cold PBS containing 0.1% NP-40. After centrifugation at 10,000 rpm for 10 s, the nuclei pellet was resuspended in 200  $\mu$ l of ice-cold PBS (without NP-40). The percent of Cy5<sup>+</sup> and the MFI of Cy5<sup>+</sup> nuclei were determined by flow cytometry.

### Statistical analysis

Data were presented as means  $\pm$  SEM from at least three replicates. Paired Student's *t* test of all data was performed. Statistical significance is defined as *P* < 0.05.

### SUPPLEMENTARY MATERIALS

Supplementary material for this article is available at <http://advances.sciencemag.org/cgi/content/full/4/11/eaau6762/DC1>

Fig. S1. Physical and functional characterization of CMP.

Fig. S2. The effect of electroporation temperature on pDNA loading efficiency.

Fig. S3. Flow cytometric histograms.

Table S1. Primers for amplification in PCR and qRT-PCR.

Table S2. Estimation of DNA copies in loaded EVs from the literature.

### REFERENCES AND NOTES

- X. Tan, Y.-Z. Gong, P. Wu, D.-F. Liao, X.-L. Zheng, Mesenchymal stem cell-derived microparticles: A promising therapeutic strategy. *Int. J. Mol. Sci.* **15**, 14348–14363 (2014).
- G. Raposo, W. Stoorvogel, Extracellular vesicles: Exosomes, microvesicles, and friends. *J. Cell Biol.* **200**, 373–383 (2013).
- A. M. Curtis, J. Edelberg, R. Jonas, W. T. Rogers, J. S. Moore, W. Syed, E. R. Mohler III, Endothelial microparticles: Sophisticated vesicles modulating vascular function. *Vasc. Med.* **18**, 204–214 (2013).
- E. Cocucci, G. Racchetti, J. Meldolesi, Shedding microvesicles: Artefacts no more. *Trends Cell Biol.* **19**, 43–51 (2009).
- M. Colombo, G. Raposo, C. Théry, Biogenesis, secretion, and intercellular interactions of exosomes and other extracellular vesicles. *Annu. Rev. Cell Dev. Biol.* **30**, 255–289 (2014).
- A. Jeyaram, S. M. Jay, Preservation and storage stability of extracellular vesicles for therapeutic applications. *AAPS J.* **20**, 1 (2017).
- X. Zhu, M. Badawi, S. Pomeroy, D. S. Sutaria, Z. Xie, A. Baek, J. Jiang, O. A. Elgamal, X. Mo, K. L. Perle, J. Chalmers, T. D. Schmittgen, M. A. Phelps, Comprehensive toxicity and immunogenicity studies reveal minimal effects in mice following sustained dosing of extracellular vesicles derived from HEK293T cells. *J. Extracell. Vesicles* **6**, 1324730 (2017).
- A. Mizrak, M. F. Bolukbasi, G. B. Ozdener, G. J. Brenner, S. Madlener, E. P. Erkan, T. Ströbel, X. O. Breakefield, O. Saydam, Genetically engineered microvesicles carrying suicide mRNA/protein inhibit schwannoma tumor growth. *Mol. Ther.* **21**, 101–108 (2013).
- Y. Akao, A. Ito, T. Itoh, S. Noguchi, Y. Itoh, Y. Ohtsuki, T. Naoe, Microvesicle-mediated RNA molecule delivery system using monocytes/macrophages. *Mol. Ther.* **19**, 395–399 (2011).
- L. Alvarez-Erviti, Y. Seow, H. Yin, C. Betts, S. Lakkh, M. J. A. Wood, Delivery of siRNA to the mouse brain by systemic injection of targeted exosomes. *Nat. Biotechnol.* **29**, 341–345 (2011).
- G. Fuhrmann, A. Serio, M. Mazo, R. Nair, M. M. Stevens, Active loading into extracellular vesicles significantly improves the cellular uptake and photodynamic effect of porphyrins. *J. Control. Release* **205**, 35–44 (2015).
- X. Zhuang, X. Xiang, W. Grizzle, D. Sun, S. Zhang, R. C. Axtell, S. Ju, J. Mu, L. Zhang, L. Steinman, D. Miller, H.-G. Zhang, Treatment of brain inflammatory diseases by delivering exosome encapsulated anti-inflammatory drugs from the nasal region to the brain. *Mol. Ther.* **19**, 1769–1779 (2011).
- Y. Zhang, L. Li, J. Yu, D. Zhu, Y. Zhang, X. Li, H. Gu, C.-Y. Zhang, K. Zen, Microvesicle-mediated delivery of transforming growth factor  $\beta$ 1 siRNA for the suppression of tumor growth in mice. *Biomaterials* **35**, 4390–4400 (2014).
- J. Wahlgren, T. De L. Karlsson, M. Brissler, F. V. Sani, E. Telemo, P. Sunnerhagen, H. Valadi, Plasma exosomes can deliver exogenous short interfering RNA to monocytes and lymphocytes. *Nucleic Acids Res.* **40**, e130 (2012).
- J. M. Cooper, P. B. O. Wiklander, J. Z. Nordin, R. Al-Shawi, M. J. Wood, M. Vitthani, A. H. V. Schapira, J. P. Simons, S. El-Andaloussi, L. Alvarez-Erviti, Systemic exosomal siRNA delivery reduced alpha-synuclein aggregates in brains of transgenic mice. *Mov. Disord.* **29**, 1476–1485 (2014).
- T. N. Lamichhane, R. S. Raiker, S. M. Jay, Exogenous DNA loading into extracellular vesicles via electroporation is size-dependent and enables limited gene delivery. *Mol. Pharm.* **12**, 3650–3657 (2015).
- M. Kanada, M. H. Bachmann, J. W. Hardy, D. O. Frimansson, L. Bronsart, A. Wang, M. D. Sylvestre, T. L. Schmidt, R. L. Kaspar, M. J. Butte, A. C. Matin, C. H. Contag, Differential fates of biomolecules delivered to target cells via extracellular vesicles. *Proc. Natl. Acad. Sci. U.S.A.* **112**, E1433–E1442 (2015).
- C. E. Thomas, A. Ehrhardt, M. A. Kay, Progress and problems with the use of viral vectors for gene therapy. *Nat. Rev. Genet.* **4**, 346–358 (2003).
- K.-R. Yu, H. Natanson, C. E. Dunbar, Gene editing of human hematopoietic stem and progenitor cells: Promise and potential hurdles. *Hum. Gene Ther.* **27**, 729–740 (2016).
- T. Schomber, C. P. Kalberer, A. Wodnar-Filipowicz, R. C. Skoda, Gene silencing by lentivirus-mediated delivery of siRNA in human CD34<sup>+</sup> cells. *Blood* **103**, 4511–4513 (2004).
- Y. Diener, M. Jurk, B. Kandil, Y.-H. Choi, S. Wild, U. Bissels, A. Bosio, RNA-based, transient modulation of gene expression in human haematopoietic stem and progenitor cells. *Sci. Rep.* **5**, 17184 (2015).
- J. M. Wiehe, P. Ponsaerts, M. T. Rojewski, J. M. Homann, J. Greiner, D. Kronawitter, H. Schrezenmeier, V. Hombach, M. Wiesneth, O. Zimmermann, J. Torzewski, mRNA-mediated gene delivery into human progenitor cells promotes highly efficient protein expression. *J. Cell. Mol. Med.* **11**, 521–530 (2007).
- M. H. Wu, D. N. Liebowitz, S. L. Smith, S. F. Williams, M. E. Dolan, Efficient expression of foreign genes in human CD34<sup>+</sup> hematopoietic precursor cells using electroporation. *Gene Ther.* **8**, 384–390 (2001).
- N. A. McNeer, J. Y. Chin, E. B. Schleifman, R. J. Fields, P. M. Glazer, W. M. Saltzman, Nanoparticles deliver triplex-forming PNAs for site-specific genomic recombination in CD34<sup>+</sup> human hematopoietic progenitors. *Mol. Ther.* **19**, 172–180 (2011).
- N. A. McNeer, E. B. Schleifman, A. Cuthbert, M. Brehm, A. Jackson, C. Cheng, K. Anandalingam, P. Kumar, L. D. Shultz, D. L. Greiner, W. Mark Saltzman, P. M. Glazer, Systemic delivery of triplex-forming PNA and donor DNA by nanoparticles mediates site-specific genome editing of human hematopoietic cells in vivo. *Gene Ther.* **20**, 658–669 (2013).
- R. Flaumenhaft, J. R. Dilks, J. Richardson, E. Alden, S. R. Patel-Hett, E. Battinelli, G. L. Klement, M. Sola-Visner, J. E. Italiano Jr., Megakaryocyte-derived microparticles: Direct visualization and distinction from platelet-derived microparticles. *Blood* **113**, 1112–1121 (2009).
- J. Jiang, D. S. Woulfe, E. T. Papoutsakis, Shear enhances thrombopoiesis and formation of microparticles that induce megakaryocytic differentiation of stem cells. *Blood* **124**, 2094–2103 (2014).
- J. Jiang, C.-Y. Kao, E. T. Papoutsakis, How do megakaryocytic microparticles target and deliver cargo to alter the fate of hematopoietic stem cells? *J. Control. Release* **247**, 1–18 (2017).
- C. Escobar, "Human megakaryocytic microparticles target murine hematopoietic stem cells to stimulate in vivo platelet biogenesis," thesis, University of Delaware (2018); <http://udspace.udel.edu/handle/19716/23576>.
- S.-i. Ohno, M. Takahashi, K. Sudo, S. Ueda, A. Ishikawa, N. Matsuyama, K. Fujita, T. Mizutani, T. Ohgi, T. Ochiya, N. Gotoh, M. Kuroda, Systemically injected exosomes targeted to EGFR deliver antitumor microRNA to breast cancer cells. *Mol. Ther.* **21**, 185–191 (2013).
- P. G. Fuhrken, C. Chen, W. M. Miller, E. T. Papoutsakis, Comparative, genome-scale transcriptional analysis of CHRF-288-11 and primary human megakaryocytic cell cultures provides novel insights into lineage-specific differentiation. *Exp. Hematol.* **35**, 476–489 (2007).
- B. J. Naughton, D. D. Han, H. H. Gu, Fluorescence-based evaluation of shRNA efficacy. *Anal. Biochem.* **417**, 162–164 (2011).

33. L. Schermelleh, R. Heintzmann, H. Leonhardt, A guide to super-resolution fluorescence microscopy. *J. Cell Biol.* **190**, 165–175 (2010).
34. J.-W. Taanman, The mitochondrial genome: Structure, transcription, translation and replication. *Biochim. Biophys. Acta* **1410**, 103–123 (1999).
35. D. R. Latulippe, A. L. Zydney, Radius of gyration of plasmid DNA isoforms from static light scattering. *Biotechnol. Bioeng.* **107**, 134–142 (2010).
36. S. Lehmusvaara, O. Rautsi, T. Hakkarainen, J. Wahifors, Utility of cell-permeable peptides for enhancement of virus-mediated gene transfer to human tumor cells. *Biotechniques* **40**, 573–576 (2006).
37. S. Panuganti, A. C. Schlinker, P. F. Lindholm, E. T. Papoutsakis, W. M. Miller, Three-stage ex vivo expansion of high-ploidy megakaryocytic cells: Toward large-scale platelet production. *Tissue Eng. Part A* **19**, 998–1014 (2013).
38. M. Aluigi, M. Fogli, A. Curti, A. Isidori, E. Gruppioni, C. Chiodoni, M. P. Colombo, P. Versura, A. D'Errico-Grigioni, E. Ferri, M. Baccarani, R. M. Lemoli, Nucleofection is an efficient nonviral transfection technique for human bone marrow-derived mesenchymal stem cells. *Stem Cells* **24**, 454–461 (2006).
39. D. A. Dean, D. D. Strong, W. E. Zimmer, Nuclear entry of nonviral vectors. *Gene Ther.* **12**, 881–890 (2005).
40. F. M. de Queiroz, A. Sánchez, J. R. Agarwal, W. Stühmer, L. A. Pardo, Nucleofection induces non-specific changes in the metabolic activity of transfected cells. *Mol. Biol. Rep.* **39**, 2187–2194 (2012).
41. R. V. Benjaminsen, M. A. Matthebjerg, J. R. Henriksen, S. M. Moghimi, T. L. Andresen, The possible "proton sponge" effect of polyethylenimine (PEI) does not include change in lysosomal pH. *Mol. Ther.* **21**, 149–157 (2013).
42. A. El-Sayed, S. Futaki, H. Harashima, Delivery of macromolecules using arginine-rich cell-penetrating peptides: Ways to overcome endosomal entrapment. *AAPS J.* **11**, 13–22 (2009).
43. H. Bai, G. M. S. Lester, L. C. Petishnok, D. A. Dean, Cytoplasmic transport and nuclear import of plasmid DNA. *Biosci. Rep.* **37**, BSR20160616 (2017).
44. J. Vacik, B. S. Dean, W. E. Zimmer, D. A. Dean, Cell-specific nuclear import of plasmid DNA. *Gene Ther.* **6**, 1006–1014 (1999).
45. E. Bianchi, R. Zini, S. Salati, E. Tenedini, R. Norfo, E. Tagliafico, R. Manfredini, S. Ferrari, c-myc supports erythropoiesis through the transactivation of KLF1 and LMO2 expression. *Blood* **116**, e99–e110 (2010).
46. E. Bianchi, J. Bulgarelli, S. Ruberti, S. Rontauroli, G. Sacchi, R. Norfo, V. Pennucci, R. Zini, S. Salati, Z. Prudente, S. Ferrari, R. Manfredini, MYB controls erythroid versus megakaryocyte lineage fate decision through the miR-486-3p-mediated downregulation of MAF. *Cell Death Differ.* **22**, 1906–1921 (2015).
47. L.-S. Wang, L. Li, L. Li, S. Chu, K.-D. Shiang, M. Li, H.-Y. Sun, J. Xu, F.-J. Xiao, G. Sun, J. J. Rossi, Y. Ho, R. Bhatia, MicroRNA-486 regulates normal erythropoiesis and enhances growth and modulates drug response in CML progenitors. *Blood* **125**, 1302–1313 (2015).
48. A. Nabbi, K. Riabowol, Rapid isolation of nuclei from cells in vitro. *Cold Spring Harb. Protoc.* **2015**, 769–772 (2015).

**Acknowledgments:** We thank J. Caplan and members of Bioimaging Center (University of Delaware) for assistance with immunofluorescence microscopy, and E. Muñoz and B. Wilson in M. Hudson's laboratory for assistance with NTA analysis. **Funding:** This project was supported by State of Delaware CAT (grant no. 15A01570), NIH (grant no. 1 S10 OD016361), and the Delaware INBRE program, with a grant from the National Institute of General Medical Sciences (NIGMS) (grant no. P20 GM103446) from the NIH and the state of Delaware. **Author contributions:** E.T.P. and C.-Y.K. designed the study and analyzed the data. C.-Y.K. carried out the experiments. E.T.P. and C.-Y.K. wrote the manuscript. **Competing interests:** The two authors are listed as inventors on a pending US/PCT patent application (publication US20170058262A1, application no. 15/308,221, PCT no. PCT/US15/31388) related to this work. The rights to the pending patent belong to the three inventors of the patent. **Data and materials availability:** All data needed to evaluate the conclusions in the paper are present in the paper and/or the Supplementary Materials. Additional data related to this paper may be requested from the authors.

Submitted 4 July 2018  
Accepted 4 October 2018  
Published 7 November 2018  
10.1126/sciadv.aau6762

**Citation:** C.-Y. Kao, E. T. Papoutsakis, Engineering human megakaryocytic microparticles for targeted delivery of nucleic acids to hematopoietic stem and progenitor cells. *Sci. Adv.* **4**, eaau6762 (2018).